Coexistence of Multiple Stacking Charge Density Waves in Kagome Superconductor CsV$_3$Sb$_5$

Qian Xiao,[1, *] Yihao Lin,[1, *] Qizhi Li,[1, *] Xiquan Zheng,[1, *] Sonia Francoual,[2] Christian Plueckthun,[2]
Wei Xia,[3, 4] Qingzheng Qiu,[1] Shilong Zhang,[1] Yanfeng Guo,[3, 4] Ji Feng,[1, 5, †] and Yingying Peng[1, 6, ‡]

[1]*International Center for Quantum Materials, School of Physics, Peking University, Beijing 100871, China*
[2]*Deutsches Elektronen-Synchrotron (DESY), Hamburg D-22607, Germany*
[3]*School of Physical Science and Technology, ShanghaiTech University, Shanghai 201210, China*
[4]*ShanghaiTech Laboratory for Topological Physics,*
ShanghaiTech University, Shanghai 201210, China
[5]*CAS Center for Excellence in Topological Quantum Computation,*
University of Chinese Academy of Sciences, Beijing 100190, China
[6]*Collaborative Innovation Center of Quantum Matter, Beijing 100871, China*
(Dated: March 13, 2023)

The recently discovered Kagome family AV$_3$Sb$_5$ (A = K, Rb, Cs) exhibits rich physical phenomena, including non-trivial topological electronic structure, giant anomalous Hall effect, charge density waves (CDW) and superconductivity. Notably, CDW in AV$_3$Sb$_5$ is evidenced to intertwine with its superconductivity and topology, but its nature remains elusive. Here, we combine x-ray scattering experiments and density-functional theory calculations to investigate the CDWs in CsV$_3$Sb$_5$ and demonstrate the coexistence of $2 \times 2 \times 2$ and $2 \times 2 \times 4$ CDW stacking phases. Competition between these CDW phases is revealed by tracking the temperature evolution of CDW intensities, which also manifests in different transition temperatures during warming- and cooling measurements. We also identify a meta-stable quenched state of CsV$_3$Sb$_5$ after fast-cooling process. Our study demonstrates the coexistence of competing CDW stackings in CsV$_3$Sb$_5$, offering new insights in understanding the novel properties of this system.

Materials with kagome nets are promising candidates for quantum spin liquid [1–3] and can support a variety of electronic orders like charge bond order, charge density wave (CDW) and unconventional superconductivity[4–6]. Recently, a new class of kagome materials AV$_3$Sb$_5$ (A = K, Rb, Cs) has entered the scene and triggered a surge of research. These materials are found to be Z_2 topological metals and show giant anomalous Hall conductivity[7–10]. More intriguingly, superconductivity transitions below $\sim$ 3 K were reported in AV$_3$Sb$_5$ [8, 11, 12]. Above the superconducting transition temperature, a CDW phase transition ranging from 78 K to 103 K was also reported [7, 8, 12, 13]. As in most unconventional superconductors, such as cuprates[14, 15] and pnictides[16], the CDW in AV$_3$Sb$_5$ seems to compete with its superconductivity [17–21]. In addition, CDW in kagome lattice has been proposed to be a chiral flux phase, which breaks the time-reversal symmetry (TRS) without spin polarization and may be related to the anomalous Hall effect [9, 10, 13, 22–24]. This TRS breaking has been found to persist into the superconductivity state, indicating an intimate relation between charge order and unconventional superconductivity [25]. Additionally, the nematic susceptibility is observed to be enhanced below CDW transition temperature by elastoresistance measurements [26]. Overall, these results indicate that the CDW in AV$_3$Sb$_5$ is intertwined with its superconductivity and topology in an intriguing way.

Of the AV$_3$Sb$_5$ family, CsV$_3$Sb$_5$ has the highest superconducting transition temperature $T_c \sim$ 2.5 K [8]. It also undergoes a CDW transition at $\sim$ 94 K with both in-plane and out-of-plane components, whose underlying mechanism remains elusive [8, 27, 28]. More strikingly, the superconducting phase diagram of CsV$_3$Sb$_5$ shows a double-dome while the CDW phase is diminished by applying pressure or doping, indicating an unusual competition between CDW and superconductivity [29–32]. Regarding the in-plane CDW, while the inverse star of David (ISD) deformation is energetically favored according to first principles calculations and as confirmed by the observation of the Shubnikov-de Haas oscillation [24, 33, 34], the star of David (SD) deformation is supported by nuclear quadrupole resonance measurements [35]. As for the out-of-plane component, in addition to the proposed $2 \times 2 \times 2$ (2c) and 1×4 modulations [13, 22, 27, 36–38], non-resonant x-ray diffraction measurements on CsV$_3$Sb$_5$ observed a unique $2 \times 2 \times 4$ (4c) CDW phase appearing below 94 K [28], which has not been reported in KV$_3$Sb$_5$ or RbV$_3$Sb$_5$. It is argued that there is only 4c CDW phase in CsV$_3$Sb$_5$ [28], which needs further experimental confirmation.

The 2c and/or 4c CDW phases may originate from different inter-layer stackings. The stacking degree of freedom in layered materials has been shown to be a powerful knob for manipulating physical properties. For example, in bilayer graphene, flat bands and superconductivity are induced by twisting two layers of non-superconducting graphene by a "magic angle" [39]. In transition metal dichalcogenides, CDW stacking is considered to be important in determining the metal-insulator transition [40, 41]. Therefore, it is important to investigate in detail the CDW phase(s) in CsV$_3$Sb$_5$,

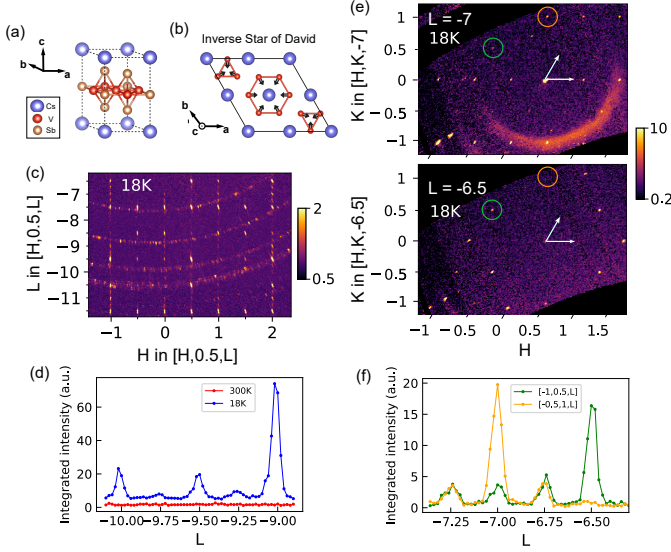in order to understand the role it plays in various electronic properties in this material.

FIG. 1: (a) Crystal structure of CsV_3Sb_5 in normal state [42]. It belongs to P6/mmm space group (No. 191) [7]. (b) Schematic plot of inverse Star of David (ISD). (c) (H, L) map of reciprocal space at $K = 0.5$ measured at 18K. The momentum axes are plotted in reciprocal length, i.e., $\mathring{A}^{-1}$. (d) L-cuts of [2.5, -3.5, L] at 300 K and 18 K, respectively. Offset is added for clarity. (e) (H, K) maps of reciprocal space at $L = -7$ (upper panel) and $L = -6.5$ (lower panel) measured at 18K. The CDW peaks highlighted by green and orange circles are related to C_6 symmetry. Their cuts along the L-direction are shown in (f). In (c)(e), the arc signals come from beryllium domes, and the intensity of data is in logscale.

In this work, we use x-ray diffraction (XRD) and resonant x-ray scattering (REXS) techniques in conjunction with density-functional theory (DFT) calculations to study the CDW phases in CsV_3Sb_5. Based on the temperature evolution of diffraction peaks, we establish the coexistence of 2c and 4c CDW phases, with different transition temperatures. The observed spectral weight transfer between 2c and 4c diffraction peaks in warming and cooling processes signals a competition between these phases. In particular, the onset temperature of 4c on cooling (~ 89 K) is found to be lower than the corresponding vanishing temperature on warming (~ 92.8 K). An intriguing quenched state due to fast cooling is observed in the warming experiment, which could have critical implications in interpreting experimental anomalies at about $60 \sim 70$ K [43–45]. By performing spatial mapping of CDW intensity using REXS, we observe that the different CDW modulations tend to exclude each other spatially further supporting the coexistence of different order parameters and competition between them. Comparison with computed diffraction patterns based on DFT calculations suggests the observed CDW structures arise from different stackings of ISD deformed

V-containing layers. Our new results clarify the stacking CDWs in CsV_3Sb_5, which is very important in understanding and controlling the topological and superconducting properties in this material.

Single crystal x-ray diffraction measurements were performed using the custom-designed x-ray instrument equipped with a Xenocs Genix3D Mo K_α (17.48 keV) x-ray source, which provides $\simeq 2.5\times10^7$ photons/sec in a beam spot size of 150 μm at the sample position [46]. Resonant x-ray scattering measurements were carried out at the beamline P09 at PETRA III, DESY (Hamburg, Germany) [47]. The single-crystalline CsV_3Sb_5 samples for the present study were grown by a self-flux growth method [46].

The structure of CsV_3Sb_5 in normal state [42] is shown in FIG. 1(a), which is comprised of alternating layers of alkali-metal and V_3Sb_5. The vanadium atoms form a perfect kagome lattice under ambient conditions [7]. After cooling from 300 K to 18 K (at a rate of 8 K/min), a cascade of CDW peaks becomes manifest at the half-integer K plane, as shown in Figure 1(c-d). Diffraction peaks are labeled by their Miller indices, (H, K, L), of the undistorted high-temperature phase. The CDW peaks are about 3 orders of magnitude weaker than the main Bragg peaks, indicating small lattice distortions. The x-ray diffraction pattern was indexed according to a hexagonal unit cell with lattice parameters $a = b \simeq 5.53\,\mathring{A}$ and $c \simeq 9.28\,\mathring{A}$ [46]. The observed CDW peaks can be classified into three categories, namely, $\mathbf{q}_1$, $\mathbf{q}_2$ and $\mathbf{q}_3$-type peaks corresponding to integer, half-integer and quarter-integer L values, respectively. For a CDW reflection, either H or K or both are half-integers owing to the in-plane 2×2 reconstruction [13, 22].

It is worth mentioning that we have not detected any reflection with a quarter integer H or K, suggesting the absence of cell quadrupling along a or b, which is consistent with previous XRD measurements [48]. Thus, our results obtained with a highly sensitive two-dimensional detector further confirm that the 1×4 modulation observed by several STM experiments may not be a bulk effect [22, 38, 48]. We also notice that C_6 symmetry is broken at low temperatures, consistent with previous works [45]. Because the CDW peaks at $\mathbf{q} = [-1, 0.5, L]$ and $[-0.5, 1, L]$ are equivalent in C_6 symmetry, however, as shown in Figure 1(e, f), they differ greatly in intensity at 18 K. Either ISD [shown in Figure 1(b)], SD distortion or order of orbital current would preserve C_6 symmetry in kagome plane. However, for a 3D CDW, the phase shift of adjacent kagome layers breaks the C_6 symmetry [24, 33, 49]. One recent measurement of polar Kerr rotation of CsV_3Sb_5 has reported the formation of twofold rotation symmetry below $T_{CDW} \sim 94$ K [50].

To further elucidate the origin of $\mathbf{q}_1$, $\mathbf{q}_2$ and $\mathbf{q}_3$-type CDW peaks, we select the CDW peaks at $\mathbf{q}_1 = [-0.5,-0.5,-9]$, $\mathbf{q}_2 = [-0.5,-0.5,-9.5]$ and $\mathbf{q}_3 = [-0.5,-0.5,-9.25]$ and trace their evolutions across transition temperatures [46].
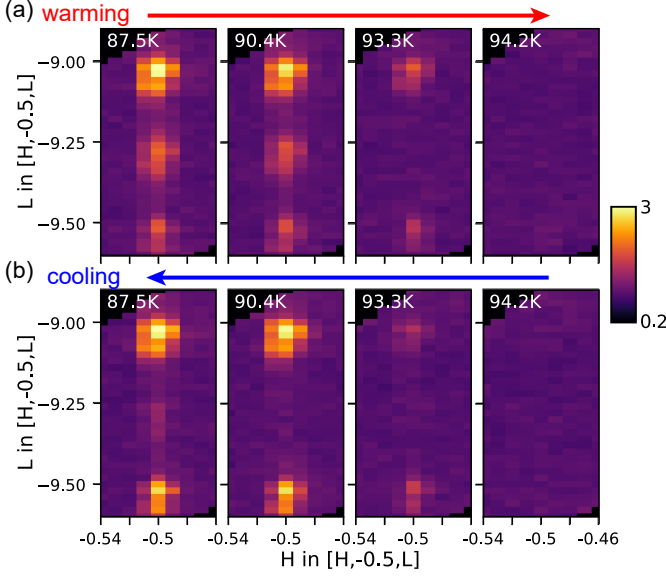
FIG. 2: Narrow (H, L) maps of reciprocal space of the CDW for a selection of temperatures. (a)(b) show temperature evolution of CDW diffractions in the warming process and cooling process, respectively. The intensity of data in the color map is in logscale.

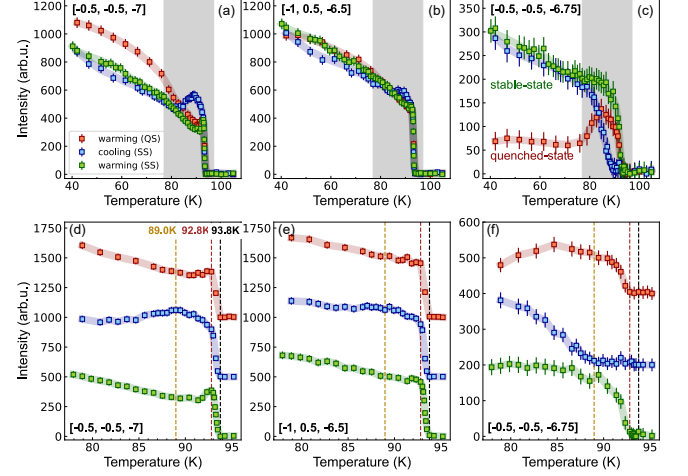

FIG. 3: (a)-(c) Temperature evolution of three CDW peaks for [-0.5, -0.5, -7], [-1, 0.5, -6.5] and [-0.5, -0.5, -6.75], respectively. The red curve is a warming process after fast cooling, referred as quenched-state (QS) as explained in the text. The blue curve is a cooling measurement and the green curve is another warming process, referred as stable-state (SS) as explained in the text. The error bars are estimated by the square root of counts. (d)-(f) Zoom-in temperature marked by the grey region to visualize three characteristic temperatures, i.e. 93.8 K, 92.8 K and 89 K. The curves are vertically shifted for clarity.

As shown in Fig. 2, the intensities of CDW peaks at $\mathbf{q}_1$ and $\mathbf{q}_2$ gradually descend with increasing temperatures and then abruptly drop to zero above $T_{\mathrm{CDW}} \sim 94$ K. Intriguingly, the $\mathbf{q}_3$-type CDW peak disappears at ~ 93 K, about 1 K lower than that of $\mathbf{q}_1$ and $\mathbf{q}_2$-CDWs. Surprisingly, in the cooling process, while $\mathbf{q}_1$ and $\mathbf{q}_2$-type CDW peaks promptly emerge below 94 K, the appearance of $\mathbf{q}_3$-type CDW peak lags until further cooling below $\sim$ 89K.

This thermal hysteresis of $\mathbf{q}_3$-type CDW peak is unexpected. As further verification, the CsV$_3$Sb$_5$ sample was subjected to multiple thermal cycling, during which the intensities of CDW peaks were recorded *in situ*, as shown in Fig. 3. The first warming process was measured after a fast cooling from room temperature to ~ 18 K at a rate of ~ 8 K/min (red curve). The measurements at each temperature point were repeated six times and summed together for better statistics. The scanning time for each temperature point was around 1.5 hours. After warming up to 105 K, we proceeded to the cool down measurement under the same conditions (blue curve), so that CDW was allowed to evolve quasi-statically. Then we performed a second warming measurement (green curve). We have tracked three CDW peaks considering their relatively strong intensity within our measured reciprocal space, indexed by [-0.5, -0.5, 7], [-1, 0.5, -6.5] and [-0.5, -0.5, -6.75] respectively. From these results we have identified a quenched-state (QS) of CDW in CsV$_3$Sb$_5$ as a consequence of the fast-cooling process, which is evidenced by the discrepancy between the two warming processes (red

and green curves). In fact, our experiments revealed that even a freezing rate of 2 K/min was too fast for the 4c CDW to establish completely, and the system would settle in a meta-stable quenched-state with weak $\mathbf{q}_3$-type CDW signals at low temperature [46]. On the other hand, a quasi-static cooling process could drive the 4c CDW into a coherent stable-state (SS) with much high intensity of $\mathbf{q}_3$-type CDW at low temperature.

For the first warming process (referred as QS), the $\mathbf{q}_3$-type CDW peak is greatly enhanced above ~ 75 K as shown in Fig. 3(c). We note that another XRD study reported the appearance of $\mathbf{q}_3$-type CDW peak above a similar temperature scale of ~ 60 K upon warming [45]. However, instead of the coexistence of $\mathbf{q}_1$, $\mathbf{q}_2$ and $\mathbf{q}_3$-type CDW peaks at 18 K that we observed, they found no signals of $\mathbf{q}_3$-type CDW peak below 60 K and argued that 4c CDW was a super-cooled phase [45]. However, we found that the intensity of the $\mathbf{q}_3$-type CDW was even stronger after quasi-static cooling, ruling out that possibility. Most intriguingly, as shown in Figure 3(d)-(f), we can identify three characteristic temperatures, i.e. 93.8 K for the onset of $\mathbf{q}_1$ and $\mathbf{q}_2$-type CDW peaks, 92.8 K for the onset of $\mathbf{q}_3$-type CDW peaks during warming process, and 89 K for the onset of $\mathbf{q}_3$-type CDW peaks during the cooling process. These multiple transition temperatures are contradicting the previous claim that the different modulations observed in CsV$_3$Sb$_5$ would originate from a unique stacking of $2 \times 2 \times 4$. The sharp tran-

sitions and hysteresis temperature behavior suggest that the CDW transitions are first-order transitions, consistent with other experiments [35, 44, 45, 51].

Moreover, our results suggest a competition between 2c and 4c CDW phases. For example, in the cooling process upon the formation of the 4c CDW phase below 89 K, the intensities of CDWs at [-0.5, -0.5, 7] and [-1, 0.5, -6.5] are suppressed after 89 K [see blue curves in Figure 3 and direct comparisons in ref. [46]]. That is to say, the onset temperature of 4c CDW at $\sim$ 89 K changes the intensity of $\mathbf{q}_1$ and $\mathbf{q}_2$-CDWs from a peak to a dip. This behavior is more pronounced in the former. We speculate this is due to the different relative contributions of 2c and 4c CDWs in $\mathbf{q}_1$ and $\mathbf{q}_2$-type CDW peaks, since the structure factors contribute differently in reciprocal space. A similar competition effect was observed in the warming process, where the disappearance of the 4c CDW phase above 92.8 K led to a peak in the intensity of CDWs at [-0.5, -0.5, 7] and [-1, 0.5, -6.5] [see green curves in Figure 3].
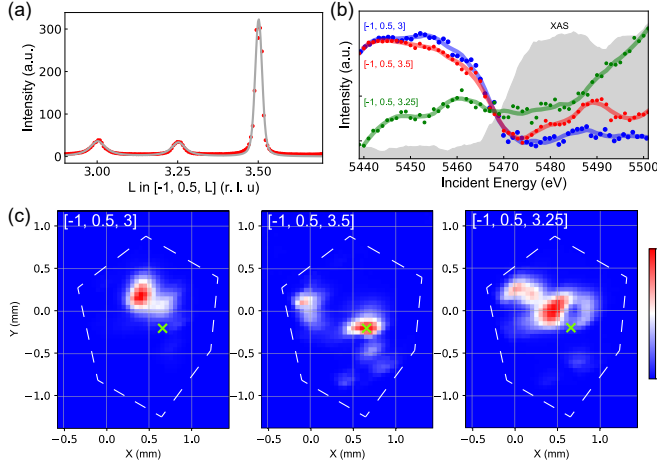

FIG. 4: (a) L-scan of [-1, 0.5, L] measured at 6 K near V K-edge (E_i = 5465 eV). The gray curve is the fit to the Voigt function. The measured position is indicated by a cross in panel (c). (b) Energy dependence for three CDW peaks at [-1, 0.5, 3], [-1, 0.5, 3.5] and [-1, 0.5, 3.25], respectively. The solid lines are guides to the eyes. The shaded area indicates the x-ray absorption spectra (XAS) at the V K-edge. (c) Spatial distributions for three CDW peaks, respectively. Data were normalized to the respective maximum intensity. The white dashed line indicates the profile of the measured sample. The markers in (c) indicate the sample position measured in (a).

The nature of the CDW phase is further elucidated using REXS at V K-edge. We selected three CDW peaks at $\mathbf{q}_1$ = [-1, 0.5, 3], $\mathbf{q}_2$ = [-1, 0.5, 3.5] and $\mathbf{q}_3$ = [-1, 0.5, 3.25] (see Fig. 4(a)) to study their energy dependence. As shown in Fig. 4(b), we observed a dip at V K-edge for all three CDW peaks. This is similar to the energy dependence of the $2 \times 2 \times 2$ CDW in TiSe$_2$, which originates from lattice displacement in CDW phase [52]. Then

we performed a spatial mapping of the intensity of the three CDW peaks at 5465 eV as shown in Fig. 4(c). Intriguingly, the $\mathbf{q}_1$, $\mathbf{q}_2$ and $\mathbf{q}_3$-CDWs seem to exclude each other spatially, rendering a single-phase scenario unlikely.
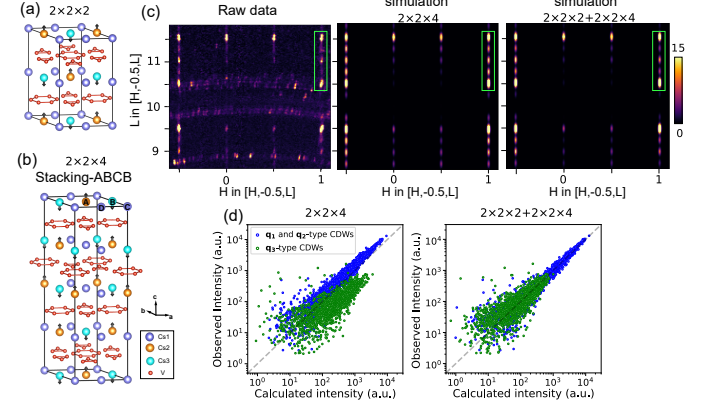

FIG. 5: (a) and (b) show the $2 \times 2 \times 2$ CDW AB-stacking pattern and the $2 \times 2 \times 4$ CDW ABCB-stacking pattern, respectively. The comparisons between the experimental XRD pattern and simulation pattern are shown in (c). The momentum axes are plotted in reciprocal length, i.e., $\mathring{A}^{-1}$. The green rectangle box highlights the difference between the experiment and the two simulations. (d) Observed X-ray diffraction intensities from 3280 CDW peaks compared to our DFT-optimized CDW structures. The blue markers indicate $\mathbf{q}_1$ and $\mathbf{q}_2$-type CDW peaks, while the green markers indicate $\mathbf{q}_3$-type CDW peaks. Considering only 4c CDW structures (left panel), and considering 2c + 4c CDW structures (right panel).

Comparison with simulated diffraction patterns lends support for the coexistence of 2c and 4c stacking CDW phases in CsV$_3$Sb$_5$. Our DFT optimization produces three types of 3D CDW structures with approximately the same energy (within 1 meV per formula unit), including one 2c CDW and two 4c CDW [46]. All structures have identical in-plane ISD deformation and differ in the stackings of V-containing layers. There are 4 translationally inequivalent Cs sites in a 2×2 supercell, denoted A, B, C, D as shown in Figure 5, and an ISD deformed V-layer is called X-stacked (X=A,B,C,D) if its contracting V-hexagon sits on the X-sites. In our DFT calculations, the SD deformation is found to be unstable and transforms spontaneously into ISD deformation when neighboring V-layers are differently stacked [33]. The stable CDW structures are the 2c supercell with AB stacking (see Fig.5(a)) and the 4c supercells with ABCB (see Fig.5(b)) and ABCD stacking [46]. Structural optimization shows that a contracting V-hexagon pulls the neighboring Cs ions toward itself. The frustration of a Cs atom in identifying with the two adjacent V layers then favors alternating stacking of the V hexagons, leading to various possible stackings.

We then fit the experimental XRD results as an incoherent superposition of the intensity of calculated CDW

structures. Since C_6 symmetry can be broken by the stacking, we consider the C_6 equivalents (three for each) in the fittings. It was argued that all CDW superlattice peaks originated from a single stacking of 4c phase [28]. Thus, we first simulated the XRD patterns considering only 4c structures, including three equivalent ABCB sequences and three equivalent ABCD sequences [more information in ref. [46]]. Figure 5(c) shows representative simulation patterns. The fitting with only the 4c structures is clearly inadequate with exaggerated $\mathbf{q}_3$-type peaks (correlation coefficient 0.80 for CDW peaks), which can be improved by including both 4c and 2c stackings in the model (correlation coefficient 0.91 for CDW peaks), as is evident from the correlation maps shown in Figure 5(d). In other words, a reasonable fit of our data is only achieved from the coexistence of 2c and 4c structures. Inclusion of the $2 \times 2 \times 1$ (1c) CDW with ISD deformation in the model produces little improvement [46]. Notably, the proposed 4c CDW structure with modulation between ISD and SD distortions [28] is inconsistent with our XRD data [46].

In summary, through systematic temperature-dependent XRD measurements, we discover the coexistence and competition of 2c and 4c CDW phases in CsV_3Sb_5 through different transition temperatures. Scanning REXS show that these modulations tend to exclude each other spatially. In conjunction with DFT calculation, our diffraction measurements reveal the microscopic origin of 2c and 4c CDW structures arising from different stackings of the "inverse star of David" structures. These results provide critical insights into the underlying CDW instability in CsV_3Sb_5 and offer a possible explanation to understand the double-peak behavior of T_c by applying pressure or doping on CsV_3Sb_5 [29, 31, 32]. The first peak of T_c may be due to the completed destruction of one stacking phase while the disappearance of both stacking CDW phases leads to the second peak of T_c. Our results reveal that the coexistent 2c and 4c CDWs are close in free energy, so external perturbations can effectively modulate the CDW phases to tune the related exotic properties. This establishes CsV_3Sb_5 as an exciting new platform for manipulating electronic properties.

---

* These authors contributed equally to this work.
† Electronic address: jfeng11@pku.edu.cn
‡ Electronic address: yingying.peng@pku.edu.cn

[1] Yan, S., Huse, D. A. & White, S. R. Spin-Liquid Ground State of the $S = 1/2$ Kagome Heisenberg Antiferromagnet. *Science* **332**, 1173–1176 (2011).

[2] Norman, M. R. Colloquium: Herbertsmithite and the search for the quantum spin liquid. *Rev. Mod. Phys.* **88**, 041002 (2016).

[3] Zhou, Y., Kanoda, K. & Ng, T.-K. Quantum spin liquid states. *Rev. Mod. Phys.* **89**, 025003 (2017).

[4] Guo, H.-M. & Franz, M. Topological insulator on the kagome lattice. *Phys. Rev. B* **80**, 113102 (2009).

[5] Ko, W.-H., Lee, P. A. & Wen, X.-G. Doped kagome system as exotic superconductor. *Phys. Rev. B* **79**, 214502 (2009).

[6] Wang, W.-S., Li, Z.-Z., Xiang, Y.-Y. & Wang, Q.-H. Competing electronic orders on kagome lattices at van hove filling. *Phys. Rev. B* **87**, 115135 (2013).

[7] Ortiz, B. R. *et al.* New kagome prototype materials: discovery of KV_3Sb_5, RbV_3Sb_5, and CsV_3Sb_5. *Phys. Rev. Materials* **3**, 094407 (2019).

[8] Ortiz, B. R. *et al.* CsV_3Sb_5: A $\mathbb{Z}_2$ Topological Kagome Metal with a Superconducting Ground State. *Phys. Rev. Lett.* **125**, 247002 (2020).

[9] Yang, S.-Y. *et al.* Giant, unconventional anomalous Hall effect in the metallic frustrated magnet candidate, KV_3Sb_5. *Science Advances* **6**, eabb6003 (2020).

[10] Yu, F. H. *et al.* Concurrence of anomalous hall effect and charge density wave in a superconducting topological kagome metal. *Phys. Rev. B* **104**, L041103 (2021).

[11] Ortiz, B. R. *et al.* Superconductivity in the $\mathbb{Z}_2$ kagome metal KV_3Sb_5. *Phys. Rev. Materials* **5**, 034801 (2021).

[12] Yin, Q. *et al.* Superconductivity and Normal-State Properties of Kagome Metal RbV_3Sb_5 Single Crystals. *Chinese Physics Letters* **38**, 037403 (2021).

[13] Jiang, Y.-X. *et al.* Unconventional chiral charge order in kagome superconductor KV_3Sb_5. *Nature Materials* **20**, 1353–1357 (2021).

[14] Ghiringhelli, G. *et al.* Long-Range Incommensurate Charge Fluctuations in (Y, Nd) Ba2Cu3O6+ x . *Science* **337**, 821–825 (2012).

[15] Chang, J. *et al.* Direct observation of competition between superconductivity and charge density wave order in $YBa_2Cu_3O_{6.67}$. *Nature Physics* **8**, 871–876 (2012).

[16] Lee, S. *et al.* Unconventional Charge Density Wave Order in the Pnictide Superconductor $Ba(Ni_{1-x}Co_x)_2As_2$. *Phys. Rev. Lett.* **122**, 147601 (2019).

[17] Song, Y. *et al.* Competition of Superconductivity and Charge Density Wave in Selective Oxidized CsV_3Sb_5 Thin Flakes. *Phys. Rev. Lett.* **127**, 237001 (2021).

[18] Wang, Q. *et al.* Charge Density Wave Orders and Enhanced Superconductivity under Pressure in the Kagome Metal CsV_3Sb_5. *Advanced Materials* **33**, 2102813 (2021).

[19] Qian, T. *et al.* Revealing the competition between charge

density wave and superconductivity in CsV_3Sb_5 through uniaxial strain. *Phys. Rev. B* **104**, 144506 (2021).

[20] Wang, N. N. *et al.* Competition between charge-density-wave and superconductivity in the kagome metal RbV_3Sb_5. *Phys. Rev. Research* **3**, 043018 (2021).

[21] Du, F. *et al.* Pressure-induced double superconducting domes and charge instability in the kagome metal KV_3Sb_5. *Phys. Rev. B* **103**, L220504 (2021).

[22] Wang, Z. *et al.* Electronic nature of chiral charge order in the kagome superconductor CsV_3Sb_5. *Phys. Rev. B* **104**, 075148 (2021).

[23] Yu, L. *et al.* Evidence of a hidden flux phase in the topological kagome metal CsV_3Sb_5. arXiv:2107.10714.

[24] Feng, X., Jiang, K., Wang, Z. & Hu, J. Chiral flux phase in the Kagome superconductor AV_3Sb_5. *Science Bulletin* **66**, 1384–1388 (2021).

[25] Mielke, C. *et al.* Time-reversal symmetry-breaking charge order in a kagome superconductor. *Nature* **602**, 245–250 (2022).

[26] Nie, L. *et al.* Charge-density-wave-driven electronic nematicity in a kagome superconductor. *Nature* **604**, 59–64 (2022).

[27] Li, H. *et al.* Observation of Unconventional Charge Density Wave without Acoustic Phonon Anomaly in Kagome Superconductors AV_3Sb_5 (A = Rb, Cs). *Phys. Rev. X* **11**, 031050 (2021).

[28] Ortiz, B. R. *et al.* Fermi Surface Mapping and the Nature of Charge-Density-Wave Order in the Kagome Superconductor CsV_3Sb_5. *Phys. Rev. X* **11**, 041030 (2021).

[29] Yu, F. H. *et al.* Unusual competition of superconductivity and charge-density-wave state in a compressed topological kagome metal. *Nature Communications* **12**, 3645 (2021).

[30] Chen, X. *et al.* Highly Robust Reentrant Superconductivity in CsV_3Sb_5 under Pressure. *Chinese Physics Letters* **38**, 057402 (2021).

[31] Chen, K. Y. *et al.* Double Superconducting Dome and Triple Enhancement of T_c in the Kagome Superconductor CsV_3Sb_5 under High Pressure. *Phys. Rev. Lett.* **126**, 247001 (2021).

[32] Oey, Y. M. *et al.* Fermi level tuning and double-dome superconductivity in the kagome metal $CsV_3Sb_{5-x}Sn_x$. *Phys. Rev. Materials* **6**, L041801 (2022).

[33] Tan, H., Liu, Y., Wang, Z. & Yan, B. Charge density waves and electronic properties of superconducting kagome metals. *Phys. Rev. Lett.* **127**, 046401 (2021).

[34] Fu, Y. *et al.* Quantum Transport Evidence of Topological Band Structures of Kagome Superconductor CsV_3Sb_5. *Phys. Rev. Lett.* **127**, 207002 (2021).

[35] Luo, J. *et al.* Possible star-of-David pattern charge density wave with additional modulation in the kagome superconductor CsV_3Sb_5. *npj Quantum Materials* **7**, 30 (2022).

[36] Liang, Z. *et al.* Three-Dimensional Charge Density Wave and Surface-Dependent Vortex-Core States in a Kagome Superconductor CsV_3Sb_5. *Phys. Rev. X* **11**, 031026 (2021).

[37] Shumiya, N. *et al.* Intrinsic nature of chiral charge order in the kagome superconductor RbV_3Sb_5. *Phys. Rev. B* **104**, 035131 (2021).

[38] Zhao, H. *et al.* Cascade of correlated electron states in the kagome superconductor CsV_3Sb_5. *Nature* **599**, 216–221 (2021).

[39] Cao, Y. *et al.* Unconventional superconductivity in magic-angle graphene superlattices. *Nature* **556**, 43–50 (2018).

[40] Influence of CDW stacking disorder on metal–insulator transition in 1T-TaS2. *Solid State Communications* **116**, 47–50 (2000).

[41] Ma, L. *et al.* A metallic mosaic phase and the origin of Mott-insulating state in 1T-TaS2. *Nature Communications* **7**, 10956 (2016).

[42] Momma, K. & Izumi, F. *VESTA3* for three-dimensional visualization of crystal, volumetric and morphology data. *Journal of Applied Crystallography* **44**, 1272–1276 (2011).

[43] Xiang, Y. *et al.* Twofold symmetry of c-axis resistivity in topological kagome superconductor CsV_3Sb_5 with in-plane rotating magnetic field. *Nature Communications* **12**, 6727 (2021).

[44] Wang, Z. X. *et al.* Unconventional charge density wave and photoinduced lattice symmetry change in the kagome metal CsV_3Sb_5 probed by time-resolved spectroscopy. *Phys. Rev. B* **104**, 165110 (2021).

[45] Stahl, Q. *et al.* Temperature-driven reorganization of electronic order in CsV_3Sb_5. *Phys. Rev. B* **105**, 195136 (2022).

[46] See Supplementary Material at...for more information about crystal synthesis, experimental details, temperature dependence of beryllium, origin of diffuse scattering signals in XRD pattern, density-functional theory calculations and fitting of experimental data.

[47] Strempfer, J. *et al.* Resonant scattering and diffraction beamline P09 at PETRA III. *Journal of Synchrotron Radiation* **20**, 541–549 (2013).

[48] Li, H. *et al.* Discovery of conjoined charge density waves in the kagome superconductor CsV_3Sb_5. *Nature Communications* **13**, 6348 (2022).

[49] Miao, H. *et al.* Geometry of the charge density wave in the kagome metal AV_3Sb_5. *Phys. Rev. B* **104**, 195132 (2021).

[50] Wu, Q. *et al.* Simultaneous formation of two-fold rotation symmetry with charge order in the kagome superconductor CsV_3Sb_5 by optical polarization rotation measurement. *Phys. Rev. B* **106**, 205109 (2022).

[51] Ratcliff, N., Hallett, L., Ortiz, B. R., Wilson, S. D. & Harter, J. W. Coherent phonon spectroscopy and interlayer modulation of charge density wave order in the kagome metal CsV_3Sb_5. *Phys. Rev. Materials* **5**, L111801 (2021).

[52] Peng, Y. *et al.* Observation of orbital order in the van der Waals material $1T-TiSe_2$. *Phys. Rev. Research* **4**, 033053 (2022).